International Journal of Aeronautical and Space Sciences (2020) 21:504–512
https://doi.org/10.1007/s42405-019-00237-7

IJASS International Journal of Aeronautical and Space Sciences

ORIGINAL PAPER

Adaptive Gliding-Guided Projectile Attitude Tracking Controller Design Based on RBF Neuro-sliding Mode Technique

Wenguang Zhang[1] · **Wenjun Yi**[1]

Received: 31 July 2019 / Revised: 9 November 2019 / Accepted: 22 November 2019 / Published online: 4 December 2019

Abstract
In this paper, a new hybrid scheme which combines radial basic function (RBF) neural network with a model following sliding mode control technique to take their common features is used to solve attitude control problem of gliding guide projectile. The attitude kinematics model described by second-order nonlinear uncertain system is divided into two single-input single-output subsystems by considering the nonlinearity as disturbance. To avoid generating high control value, the coupled inputs are kept as one nominal input instead of being included in lumped uncertainties. The uncertainties in the plant are cancelled by an adaptive RBF neural networks estimator, which is designed based on Lyapunov theory. To verify the effectiveness of the proposed control strategy, attitude tracking control experiments are simulated under strong internal and external disturbances.

Keywords Model following control · Sliding mode control · Tracking differentiator · RBF neural network · Attitude tracking control

1 Introduction

Traditional ballistic missiles and flying missiles have not been able to achieve full penetration. Therefore, with the improvement of missile defence system, the new missile called boost-gliding-guided projectile which combines the advantages of both ballistic missiles and flying missiles is developed [1]. This kind of missile is launched by barrel weapon. Once coming through the muzzle, it opens the tail wing, which enables it to spin at a specified speed and to maintain stable fight. After a few seconds, the small rocket booster engine on the missile begins working to assist the missile in climbing. Once the rocket shuts down, the missile detect system starts to work. When the missile reaches somewhere near the vertex, the duck rudders are opened. Then the guiding system continuously adjusts the deflections of the rudders to control the attitude of the projectile. By this way, the range is extended and precise strike can be achieved [2]. Due to the rotating characteristics of the projectile and some other factors, such as the delay between the control instructions and the response of the rudder system, there is significant cross coupling between the yaw channel and the pitch channel. What's more, the gliding-guided projectile control model which is always constructed under some assumptions differs from the actual one, and the projectile suffers from uncertain disturbance and dynamic parameters perturbation in flight. In other words, the attitude control problem studied in this paper can be classified as the control problem of nonlinear multiple-input multiple-output (MIMO) uncertain system. To deal with such problem, researchers have proposed many methods, such as feedback linearization method, fuzzy method, variable structure method [3–10] and so on. Among them, variable structure method is widely used to solve nonlinear control problems [11–15], for its merits of simplicity in implementation, fast dynamic response, and robustness against parameter variations. However, traditional sliding mode control suffers from the chattering problem [16]. As a remedy to this drawback, higher order sliding mode control approach is proposed [17–20]. Furthermore, to cope with the uncertain terms in model plant, estimator should be used. Artificial neural network (ANN) is an efficient tool to estimate disturbance due to its major advantages such as strong self-learning skills, and powerful ability to map nonlinear system. Usually, ANNs adopt Hebb or learning rule to adjust weights of networks [21], but that can only guarantee the system is convergent around the ideal value. So, researchers propose online adap-

✉ Wenguang Zhang
wgz8911@163.com

[1] National Key Laboratory Transient Physics, Nanjing University of Science and Technology , Nanjing 210094, China

tive neural network [22–26], which is based on Lyapunov stable theory, to ensure the stability of closed-loop system.

In general, estimator is assigned to figure out the uncertainties in plant parameters, as well as coupling inputs and external disturbance [27,28].

In this paper, we take the gliding guided missile as a research object, and a composite control strategy is proposed to solve the problem of cross coupling and uncertain disturbance. Specifically, the coupled control inputs are regarded as a single channel input, while the rest part of the plant is treated as lumped uncertainty. Model following control approach is adopted in the framework of full-order sliding mode control, in this way, it is feasible to get the desired control quality. The uncertainties are cancelled by an adaptive RBF neural network estimator, and the convergence of system is demonstrated through Lyapunuov stable theory. The effectiveness of the control method proposed in this paper is verified through simulation. Simulation results show that the controller proposed can achieve high control precision, and is robust to internal and external disturbances.

The rest of this study is organized as follows. In Sect. 2, the problem to be solved is described. In Sect. 3, the decoupling control is designed based on model following SMC and an adaptive RBF network estimator, and the stability of system is proved. In Sect. 4, comparison simulation is performed, and the improved attitude controller is given.

2 Gliding-Guided Projectile Attitude Kinematics Model

Consider that the gliding-guided projectile is gliding along a short flight path, assuming the flight speed and rotational speed of the projectile are constant, and neglect the variation of the dynamic pressure and Mach number as well as other physical parameters. Under the assumption that the attack angle and side slip angle are small, the attitude kinematics model of the gliding-guided projectile can be constructed as [23]

$$\begin{cases} \dot{\theta} = a_1\alpha - a_2\beta + a_3\delta_z \\ -\dot{\varphi}\cos\theta = a_1\beta - a_2\alpha - a_3\delta_y \\ \ddot{\vartheta} = b_1\alpha - b_2\beta + b_4\delta_z - b_3\dot{\vartheta} + b_5\cos\vartheta\cdot\dot{\psi} \\ \ddot{\psi}\cos\vartheta = b_1\beta + b_2\alpha + b_4\delta_y - b_3\cos\vartheta\cdot\dot{\psi} - b_5\dot{\vartheta}, \end{cases} \tag{1}$$

where α represents angle-of-attack; β represents side slip angle; θ and φ are trajectory inclination angle and trajectory deflection angle ,respectively; ϑ and ψ are angle of pitch and angle of yaw, respectively; δ_z and δ_y are equivalent rudder angle of pitch channel and equivalent rudder angle of yaw channel, respectively; a_i and b_i are kinetic coefficients, $a_1 = \frac{QS}{mv}(C_L^\alpha + C_L^\delta)$,$a_2 = \frac{QS}{mv}C_\mu''(\dot{\gamma}d/v)$,$a_3 = \frac{QS}{mv}(C_L^\alpha$,$b_1 = \frac{QS}{E}(m_z' + m_\sigma')$,$b_2 = \frac{QSl\dot{\gamma}D}{Ev}m_y''$,$b_3 = \frac{QSlD}{Ev}m_{zz}'$,$b_4 = \frac{QSl}{E}m_\sigma'$,$b_5 = \frac{C\dot{\gamma}}{E}$, where m is mass, v is velocity, D is missile diameter, S and l are characteristic area and characteristic length, respectively, Q is dynamic pressure, $\dot{\gamma}$ is rotational speed of the missile, E and C are equatorial damping coefficient and polar damping coefficient, respectively, C_L^α and C_L^δ are derivation of lift induced by missile and that induced by canard, respectively, C_μ'' and m_y'' are Magnus force and the derivation of Magnus moment, respectively, m_z' is derivation of the static moment, m_{zz}' is the derivation of equatorial damping moment, and m_σ' is the derivation of control moment induced by canard.

When studying the attitude control problem of the projectile, we can think the attitude change speed is faster than the change speed of velocity vector direction of projectile center of mass [24]. Without loss of generality, we assume that $\dot{\vartheta} \approx \dot{\alpha}$, $\dot{\varphi} \approx \dot{\beta}$. From (1) and the assumption of $\alpha = \vartheta - \theta$, $\beta = (\psi - \varphi)\cos\theta$, $\cos\theta \approx \cos\vartheta$, we obtain

$$\begin{cases} \ddot{\beta} = -k_1\dot{\beta} - k_2\dot{\alpha} + k_3\beta + k_4\alpha \\ \qquad + k_5\delta_y - k_6\delta_z - k_7\dot{\delta}_y \\ \ddot{\alpha} = -k_1\dot{\alpha} - k_2\dot{\beta} + k_3\alpha - k_4\beta \\ \qquad + k_5\delta_z - k_6\delta_y - k_7\dot{\delta}_z, \end{cases} \tag{2}$$

where $k_1 = b_3 + a_1$, $k_2 = b_5 + a_2$, $k_3 = b_1 - b_3a_1 + b_5a_2$, $k_4 = b_2 - b_3a_2 - b_5a_1$, $k_5 = b_4 - b_3a_3$, $k_6 = b_5a_3$, $k_7 = a_3$. Here the steering gear system is considered to be second order, the steady output of equivalent rudder deflection of a spinning gliding missile is denoted as [25]:

$$\begin{bmatrix} \delta_y \\ \delta_z \end{bmatrix} = k_s k_r \begin{bmatrix} \cos\gamma_d & \sin\gamma_d \\ -\sin\gamma_d & \cos\gamma_d \end{bmatrix}, \tag{3}$$

where

$$\begin{cases} k_s = \dfrac{1}{\sqrt{(1 - T_s^2\dot{\gamma}^2)^2 + (2\mu_s T_s\dot{\gamma})^2}} \\ k_r = \tau\dot{\gamma} + \arccos\dfrac{1 - T_s^2\dot{\gamma}^2}{\sqrt{(1 - T_s^2\dot{\gamma}^2)^2 + (2\mu_s T_s\dot{\gamma})^2}}, \end{cases} \tag{4}$$

where δ_{yc} and δ_{zc} are equivalent rudder deflect angle control signal for pitching channel and yaw channel, respectively, k_s is gain of canard, T_s is time constant of steer gear system, μ_s is system damping ratio, τ is delay time, γ_d is delay phase angle.

By omitting $\dot{\delta}_y$ and $\dot{\delta}_z$, from (1), (2) and (3), we get

$$\begin{cases} \ddot{\beta} = -k_1\dot{\beta} - k_2\dot{\alpha} + k_3\beta + k_4\alpha \\ \qquad + \kappa_5\delta_y c - \kappa_6\delta_z c \\ \ddot{\alpha} = -k_1\dot{\alpha} - k_2\dot{\beta} + k_3\alpha - k_4\beta \\ \qquad + \kappa_5\delta_z c + \kappa_6\delta_y c, \end{cases} \tag{5}$$

where

$$\begin{aligned}\kappa_5 &= k_5 k_s k_r \cos\gamma_d - k_6 k_s k_r \sin\gamma_d,\\ \kappa_6 &= k_5 k_s k_r \sin\gamma_d + k_6 k_s k_r \cos\gamma_d.\end{aligned} \tag{6}$$

Taking parameter variation and external disturbance into consideration, with denoting $u_1 = \delta_{yc}, u_2 = \delta_{zc}, x_1 = \beta, x_2 = \dot{\beta}, x_3 = \alpha, x_4 = \dot{\alpha}$, we get

$$\begin{cases}\dot{x}_1 = & x_2\\ \dot{x}_2 = & f_1(x,t) + \Delta f_1(x,t) + g_{11}(x,t)u_1 + \Delta g_{11}(x,t)u_1\\ & + g_{12}(x,t)u_2 + \Delta g_{12}(x,t)u_2 + d_1\\ \dot{x}_3 = & x_4\\ \dot{x}_4 = & f_2(x,t) + \Delta f_2(x,t) + g_{21}(x,t)u_1 + \Delta g_{21}(x,t)u_1\\ & + g_{22}(x,t)u_2 + \Delta g_{22}(x,t)u_2 + d_2,\end{cases} \tag{7}$$

where $f_1(x,t) = -k_1x_1 - k_2x_2 + k_3x_1 + k_4x_3$, $f_2(x,t) = -k_1x_4 + k_2x_2 + k_3x_3 - k_4x_1$, $g_{11} = \kappa_5, g_{12} = -\kappa_6, g_{21} = \kappa_5$, and $g_{22} = \kappa_6$.

In (7), we can see that x_1, x_2 are all influenced by the coupled inputs, which makes the control problem very complicating. To solve this problem, we denote a nominal input vector $U = \begin{bmatrix}U_1 & U_2\end{bmatrix}^T$, and it satisfies

$$U = F\begin{bmatrix}u_1\\ u_2\end{bmatrix} = \begin{bmatrix}g_{11} & g_{12}\\ g_{21} & g_{22}\end{bmatrix}\begin{bmatrix}u_1\\ u_2\end{bmatrix}. \tag{8}$$

The rest part beside control U in (7) is treated as a lumped uncertainty, which is denoted as

$$\begin{aligned}d &= \begin{bmatrix}d_p\\ d_q\end{bmatrix}\\ &= \begin{bmatrix}f_1(x,t) + \Delta f_1(x,t) + g_{11}(x,t)u_1 + \Delta g_{11}(x,t)u_1\\ \quad + g_{12}(x,t)u_2 + \Delta g_{12}(x,t)u_2 + d_1\\ f_2(x,t) + \Delta f_2(x,t) + g_{21}(x,t)u_1 + \Delta g_{21}(x,t)u_1\\ \quad + g_{22}(x,t)u_2 + \Delta g_{22}(x,t)u_2 + d_2\end{bmatrix}.\end{aligned} \tag{9}$$

Then (7) can be transformed into two decoupled subsystems:

$$\begin{aligned}\dot{x}_p &= A_p x_p + B_p U_1 + B_p d_p,\\ y_p &= x_1,\end{aligned} \tag{10}$$

and

$$\begin{aligned}\dot{x}_q &= A_q x_q + B_q U_2 + B_q d_q,\\ y_q &= x_3,\end{aligned} \tag{11}$$

where $x_p = \begin{bmatrix}x_1 & x_2\end{bmatrix}^T$, $x_q = \begin{bmatrix}x_3 & x_4\end{bmatrix}^T$, $A_p = \begin{bmatrix}0 & 1\\ 0 & 0\end{bmatrix}^T$, $B_p = \begin{bmatrix}0 & 1\end{bmatrix}^T$, $A_q = \begin{bmatrix}0 & 1\\ 0 & 0\end{bmatrix}^T$, $B_q = \begin{bmatrix}0 & 1\end{bmatrix}^T$, and $y = \begin{bmatrix}y_p & y_q\end{bmatrix}^T$ are output signals.

The object is to design a control input U so as to drive the output vector $y = \begin{bmatrix}y_p & y_q\end{bmatrix}^T$ to follow the control command $y_c = \begin{bmatrix}y_{1c} & y_{2c}\end{bmatrix}^T = \begin{bmatrix}y_{pc} & y_{qc}\end{bmatrix}^T$ in spite of the uncertainties and external disturbances.

3 Design of Control

In this section, we design a controller based on model following control method in the framework of a full-order sliding mode control suggested in [32]. Besides, the uncertainties are compensated by an adaptive RBF neural network estimator. Because the subsystems (10), (11) have similar forms, we only take(10) as an example to display the design process of control.

3.1 Model Following Control with Full-Order Sliding Mode

Let

$$\dot{x}_{pm} = A_{pm}x_{pm} + B_{pm}y_{1c}, \tag{12}$$

be a stable model satisfying certain structural conditions stated by the following assumption:

Assumption 1 A_{pm} and B_{pm} in (12) satisfy

$$A_p - A_{pm} = B_p L, \quad B_{pm} = B_p M, \tag{13}$$

where L and M are known matrixes.

Define a sliding surface [25]

$$\sigma = B_p^T x_p + z_p, \quad z_p(0) = -B_p^T x_p(0), \tag{14}$$

where

$$\dot{z}_p = -B_p^T A_{pm} x_p - B_p^T B_{pm} y_{1c}, \tag{15}$$

where the chosen sliding surface offers the full-order sliding mode, i.e., the order of the sliding surface is identical to the origin system's [32]. The dynamics of auxiliary z_p provides perfect model following once σ goes to zero and the subsystem (10) tracks the desired model dynamic given by (12) [28]. Differentiating (14) and using (10) with (15) give

$$\begin{aligned}\dot{\sigma} &= B_p^T A_p x_p + B_p^T B_p U_1 + B_p^T B_p d_p - B_p^T A_{pm} x_p \\ &\quad - B_p^T B_{pm} y_{1c} \\ &= B_p^T L x_p + B_p^T B_p U_1 - B_p^T B_p M y_{1c} + \\ &\quad B_p^T B_p d_p.\end{aligned} \tag{16}$$

Let the control U_1 be split as

$$U_1 = U_{\text{eq}} + U_n, \tag{17}$$

where the equivalent control U_{eq} is put in charge of the known dynamics and U_n takes care of the lumped uncertainty in (16). Choosing

$$U_{\text{eq}} = -L x_p + M y_{1c} - (B_p^T B_p)^{-1} k_p \sigma, \tag{18}$$

where k_p is a positive constant. From (16), (17), and (18), we obtain

$$\dot{\sigma} = -k_p \sigma + B_p^T B_p U_n + B_p^T B_p d_p. \tag{19}$$

Next, the compensator U_n will be designed.

3.2 Design of Adaptive Compensator

The uncertainties in parameter and external disturbance are the main factors influencing the existence of the sliding mode for σ. To neglect the uncertain term in (19), RBF neural network is used to design an adaptive compensator.

The compensator U_n is designed as

$$U_n = -\rho, \tag{20}$$

where ρ is the upper bound of the uncertain term in (19) which is hard to be predicted. Thus, we use RBF neural network to estimate its value dynamically. $\chi = \begin{bmatrix} x_1 & x_2 \end{bmatrix}^T$ is the input vector of RBF network, the estimation of ρ is defined as

$$\hat{\rho} = \hat{w}^T \varphi(\chi), \tag{21}$$

where $\hat{w}^T$ is the weight for RBF network and $\varphi(\chi)$ is chosen to be Gauss function with the form

$$\varphi(\chi) = \exp\left(-\frac{\|\chi - c_i\|^2}{b_i^2}\right), \quad i = 1, 2, \ldots, n, \tag{22}$$

where c_i denotes the center of the ith neuron, b_i denotes the width of the ith neuron, and n denotes the number of neurons. Therefore, the compensator using RBF network for estimating the upper bound of the uncertainties is designed as follows:

$$U_n = -\hat{\rho}. \tag{23}$$

From (19) and (23), we can have

$$\dot{\sigma} = -k_p \sigma + B_p^T B_p (d_p - \hat{\rho}). \tag{24}$$

Because

$$\begin{aligned} d_p - \hat{\rho} &= d_p - \rho^* - \hat{\rho} \\ &= \eta + w^* \varphi(\chi) - \hat{w} \varphi(\chi) \\ &= \eta + \tilde{w} \varphi(\chi), \end{aligned} \tag{25}$$

where $\eta = d_p - \rho^*$ represents approximate error of the optimal RBF network, the w^* represents the optimal weight for RBF network, $\rho^* = w^* \varphi(\chi)$ represents the optimal output of RBF network, and $\tilde{w} = w^* - \hat{w}$. Then (24) becomes

$$\dot{\sigma} = -k_p \sigma + B_p^T B_p (\eta + \tilde{w} \varphi(\chi)). \tag{26}$$

Lyapunov function is defined as $V = \frac{1}{2}\sigma^2 + \frac{1}{2N}\tilde{w}^2$, and weight value of the RBF network is adjusted online by adaptive algorithm. Choosing $\dot{\hat{w}} = N B_p^T B_p \sigma \varphi(\chi)$, where N is positive constant, the following is derived:

$$\begin{aligned} \dot{V} &= \sigma \dot{\sigma} - N^{-1} \tilde{w} \dot{\hat{w}} \\ &= \sigma(-k_p \sigma + B_p^T B_p (\eta + \tilde{w} \varphi(\chi))) - B_p^T B_p \sigma \tilde{w} \varphi(\chi) \\ &= -k_p \sigma^2 + B_p^T B_p \sigma \eta \\ &\le -k_p |\sigma|^2 + B_p^T B_p |\sigma| \eta \\ &= -k_p |\sigma| (|\sigma| - k_p^{-1} B_p^T B_p \eta). \end{aligned} \tag{27}$$

To lead $\dot{V} \le 0$, k_p should satisfy $k_p \ge \frac{B_p^T B_p \eta}{|\sigma|}$. If and only if $|\sigma| = k_p^{-1} B_p^T B_p$, $\dot{V} = 0$. When $\dot{V} = 0$, $|\sigma| \equiv k_p^{-1} B_p^T B_p \eta$. According to LaSalle invariance principle [33], system (14) is asymptotic stable, which means $|\sigma| \to k_p^{-1} B_p^{-1} \eta$ when $t \to \infty$. Besides, the convergence rate depends on k_p.

Due to $V \ge 0$, $\dot{V} \le 0$, V is bounded when $t \to \infty$. Therefore, $\tilde{w}$ is bounded. It is noted that the larger the k_p is, the smaller approximate error the optimal RBF network has, which will make σ have a smaller convergence radius and as a result, the effect of model tracking will be improved.

4 Simulation and Results

In this section, the validity of the proposed control scheme is demonstrated by applying it to the attitude control problem of a certain type of gliding guided projectile.

4.1 Simulation Parameters

The parameters of the gliding-guided projectile are given in Table 1.

Table 1 Parameters for a gliding-guided projectile

b_1/s^{-2}	b_2/s^{-2}	b_3/s^{-2}	b_4/s^{-2}	b_5/s^{-2}
−129.4	0	0.191	97.519	2.286
α_1/s^{-1}	α_2/s^{-1}	α_3/s^{-1}	$\dot{\gamma}$(r/s)	τ/s
0.287	0	0.062	10	0.015
k_s	T_s/s	μ_s	$\delta_{max}/^\circ$	$\dot{\delta}_{max}/(rad/s)$
1	1/150	0.7	20	200

Table 2 The parameters of controller

Parameter	N	k_p	k_q
Value	21	200	200

The attitude angle tracking command is given by

$$\begin{cases} \beta_c = y_{1c} = \begin{cases} 1^\circ, & 1 < t \le 2 \\ -1^\circ, & t > 2 \\ 5^\circ, & t \le 1.6 \end{cases} \\ \alpha_c = y_{2c} = \begin{cases} 4^\circ, & 1.6 < t \le 3 \\ 7^\circ, & t > 3. \end{cases} \end{cases} \tag{28}$$

The controller parameters are set as Table 2 shows. The initial value of weight w of RBF network is $[0.1\ 0.1\ 0.1\ 0.1\ 0.1]^T$, $c_p = [-1^\circ\ \ -0.5^\circ\ \ 0^\circ\ \ 0.5^\circ\ \ 1^\circ]^T$, $c_q = [-7^\circ\ \ -3.5^\circ\ \ 0^\circ\ \ 3.5^\circ\ \ 7^\circ]^T$, and $b = 2$.

Since the second-order system in (7) is split into two subsystems, $A_p = A_q = \begin{bmatrix} 0 & 1 \\ 0 & 0 \end{bmatrix}$, $B_p = B_q = [0\ 1]^T$.

The reference model to be followed is chosen as

$$\dot{x}_m = A_m x_m + B_m u_m, \tag{29}$$

where $A_m = \begin{bmatrix} 0 & 1 & 0 & 0 \\ -400 & -36.6 & 0 & 0 \\ 0 & 0 & 0 & 1 \\ 0 & 0 & -200 & -24.6 \end{bmatrix}$.

Besides, $B_m = \begin{bmatrix} 0 & 0 \\ 400 & 0 \\ 0 & 0 \\ 0 & 200 \end{bmatrix}$. The initial values for the plant and model are

$$\begin{aligned} x(0) &= [0.01\ 0\ 0.01\ 0]^T, \\ x_m(0) &= [0\ 0\ 0\ 0]^T. \end{aligned} \tag{30}$$

Next, we perform two kinds of experiments: 1, the closed-loop system of attitude suffers from strong internal and external disturbance; 2, Monte Carlo experiments with parameters variation.

4.2 Attitude Decoupling Control Simulation Under Strong Internal and External Disturbances

4.2.1 Comparison Experiment Between the Proposed Decoupling Controller and ESO-PD Controller

In this simulation, severe disturbances are considered. $\Delta f_1(x,t)$, $\Delta f_2(x,t)$, $\Delta g_{11}(x,t)$, $\Delta g_{12}(x,t)$, $\Delta g_{21}(x,t)$, and $\Delta g_{22}(x,t)$ are 40% uncertainty in $f_1(x,t)$, $f_2(x,t)$, $g_{11}(x,t)$, $g_{12}(x,t)$, $g_{21}(x,t)$ and $g_{22}(x,t)$, respectively. The external disturbance vector is

$$d = \begin{bmatrix} 4x_1 \sin(0.5t) \\ 3x_3 \cos(t) \end{bmatrix}. \tag{31}$$

For performance comparison, the ESO (extended state observer) − PD (proportional and differential) controller proposed in [10] is also simulated under the same conditions.

Simulation results are shown as Fig. 1. From Fig. 1a, b, we can see that both the proposed method and ESO-PD method can track the desired output with smooth trajectories. It should be noted that the proposed method responses are relative more quick than ESO-PD method. As shown in Fig. 1c, d, the sliding surfaces start from zero point and have a smooth trajectory with no chattering phenomenon, which demonstrates the characteristics of full-order SMC. And this can be verified from the attitude tracking trajectory with reference model attitude as shown in Fig. 1e, f. Figure 1g, h shows the estimation of lumped uncertainties. A deviation from the trajectory of lumped uncertainties is observed whenever there is a step change in α and β. But the output of the adaptive compensator is able to response to the change timely. From Fig. 1i, j, we can observe that ESO-PD method always demands much larger control commands to response to the change of attitude angle tracking instructions. Despite that, the controller proposed in this paper performs better in dealing with the coupling terms contained in (7), which has been demonstrated by Fig. 1a, b. Figure 1k, l shows the equivalent canard angle. It should be noted that both of the two methods change sharply at certain time, which may do harm to the actuator. To prevent this phenomenon, it is essential to arrange a transition process for the reference inputs. The method is described in the following.

4.2.2 Tracking Differentiator (TD)

In this paper, a discrete tracking differentiator (TD) is used to provide transition process for $y_{ic}, i = 1, 2$:

$$\begin{cases} v_{i1}(k+1) = v_{i1}(k) + h v_{i2}(k) \\ v_{i2}(k+1) = v_{i2}(k) - rhsat(v_{i1}(k) - y_{ic}(k), \\ \qquad\qquad v_{i2}(k), r_0, h_0), \end{cases} \tag{32}$$

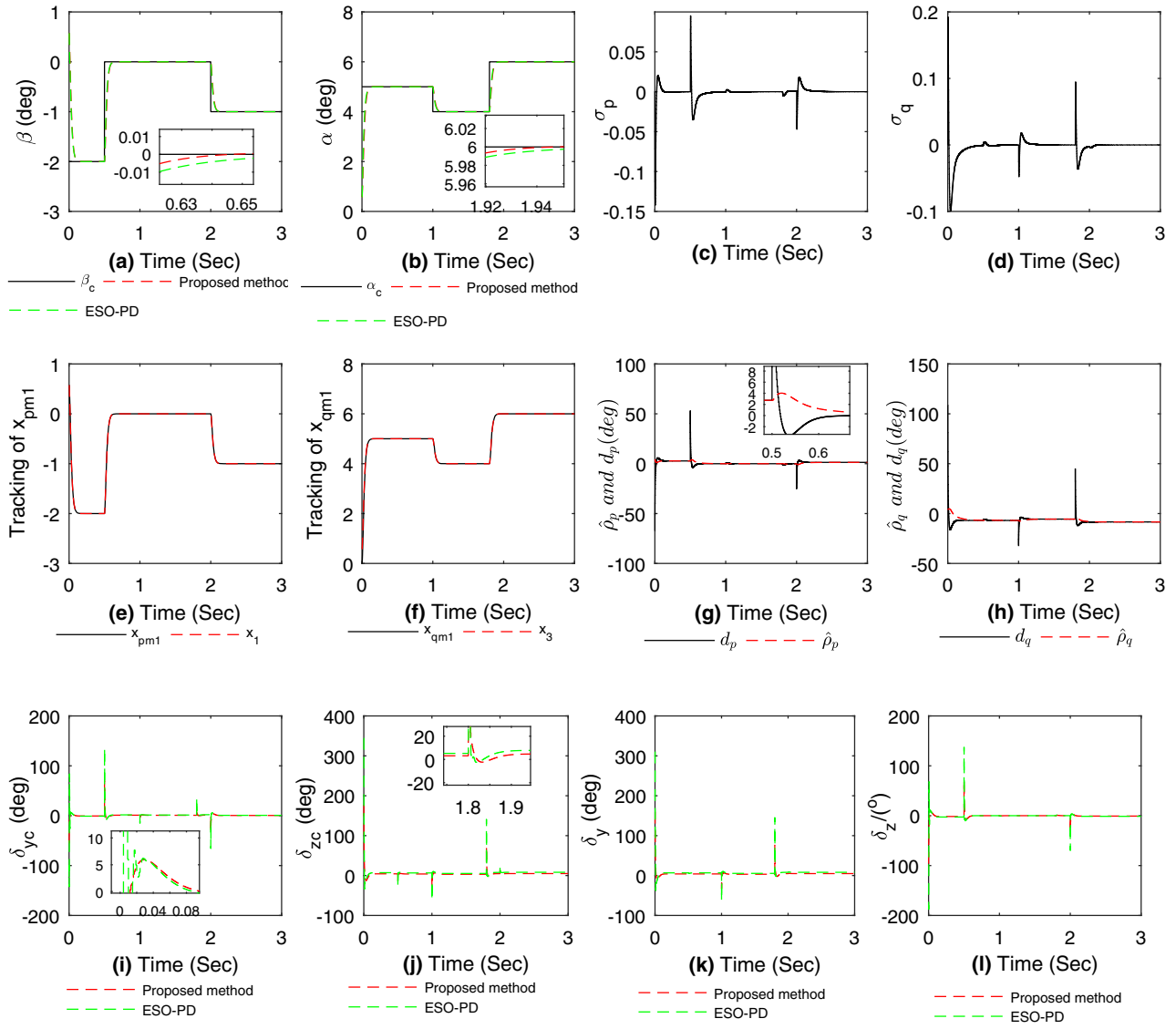

Fig. 1 Comparison analysis between the proposed decoupling controller and ESO-PD controller: **a** tracking effect of yaw commands; **b** tracking effect of pitch commands; **c** sliding surface σ_p; **d** sliding surface σ_q; **e** tracking of x_{pm}; **f** tracking of x_{qm}; **g** lumped uncertainty estimation of d_p; **h** lumped uncertainty estimation of d_q; **i**equivalent canard angle commands in yaw channel; **j** equivalent canard angle commands in pitch channel; **k** equivalent canard angle in yaw channel; **l** equivalent canard angle in yaw channel

where v_{i1} represents transition signal, whose differential is v_{i1}, h is integration step, $v_{i1}(k)$, $v_{i2}(k)$ and $y_{ic}(k)$ denotes their states at $T = kh$, h_0 is filter factor, which plays an important role in noise suppression. Here, it is not needed to filter the control command, so $h_0 = h$. r_0 represents speed factor, and it is used to adjust tracking speed. Let T_d represent the time of the transition process, then the following equation holds:

$$r_0 = 4(y_{ic} - v_{i1}(t_0))/T_d^2, \tag{33}$$

where $v_{i1}(t_0)$ represents the initial value of v_{i1}.

In (32), $sat(\xi_1, \xi_2, r, h)$ is denoted as

$$\begin{cases} a = rh, \quad a_1 = ha, \quad z = \xi_1 + h\xi_2 \\ g = \begin{cases} v_{i2} - sign(z)\dfrac{r(h - \sqrt{\frac{8|z|}{r} + h^2})}{2}, & |z| \geq a_1 \\ v_{i2} + \dfrac{z}{h}, & |z| < a_1 \end{cases} \\ sat(\xi_1, \xi_2, r, h) = a, \end{cases} \tag{34}$$

where $sign(\cdot)$ denotes the standard sign function.

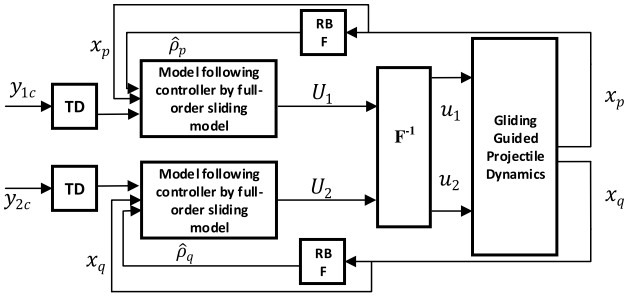

Fig. 2 The overview attitude decoupling control of the gliding guided projectile

4.2.3 The Overview Attitude Decoupling Control of the Gliding-Guided Projectile

The attitude decoupling control of the gliding guided projectile based on full-order sliding mode control and adaptive RBF network compensator is depicted as Fig. 2. As shown, TD provides gradient signal for the reference inputs y_{1c} and y_{2c}, by which the large jumping phenomenon and saturation of the control signal is avoided. Model following controllers are designed in the framework of full-order sliding mode control. What's more, an adaptive compensator based on RBF network is proposed to enhance system robustness against parameter variation and external disturbance.

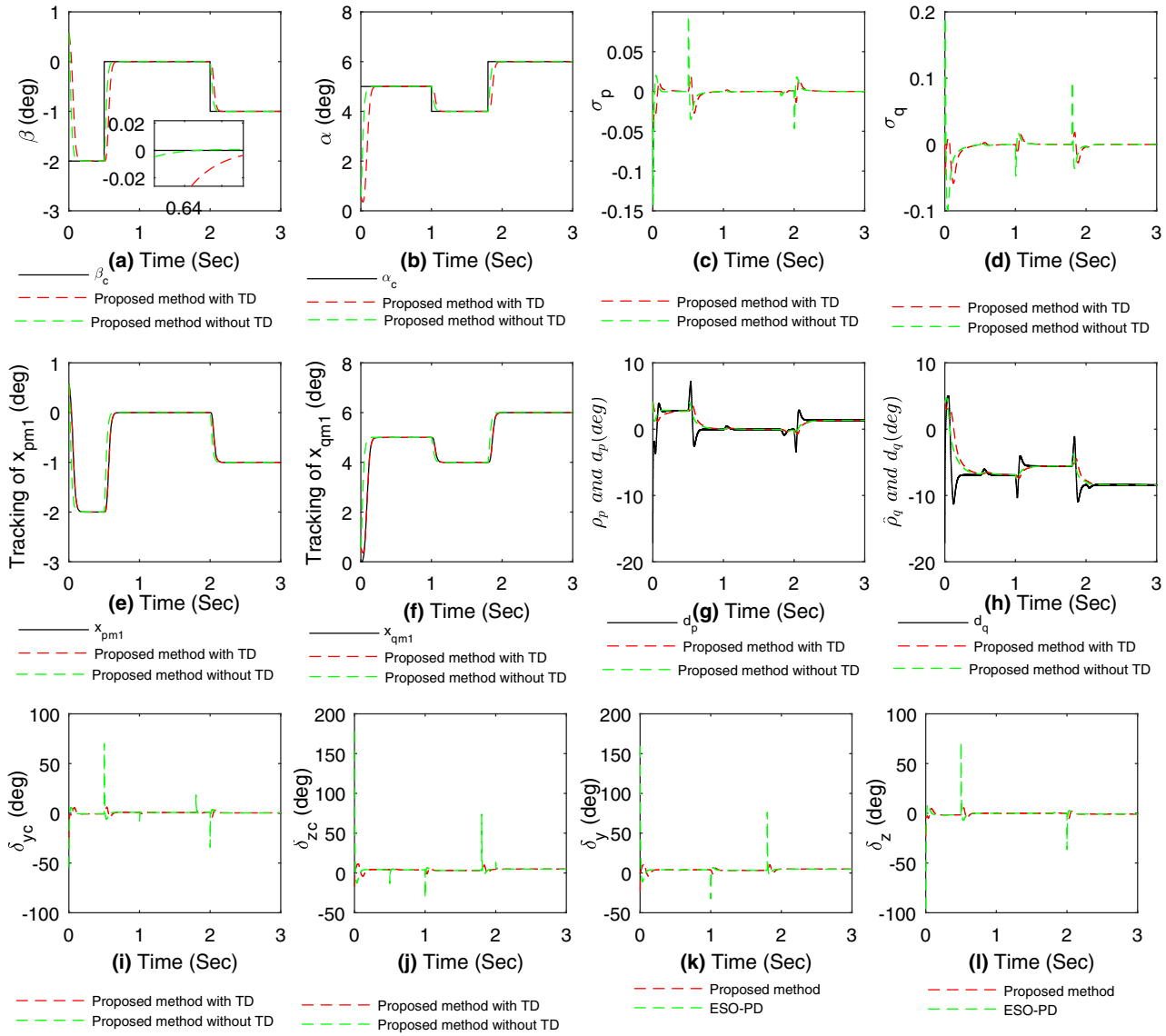

Fig. 3 Comparison analysis between the improved controller and proposed method without TD: **a** tracking effect of yaw commands; **b** tracking effect of pitch commands; **c** sliding surface σ_p; **d** sliding surface σ_q; **e** tracking of x_{pm}; **f** tracking of x_{qm}; **g** lumped uncertainty estimation of d_p; **h** lumped uncertainty estimation of d_q; **i** equivalent canard angle commands in yaw channel; **j** equivalent canard angle commands in pitch channel; **k** equivalent canard angle in yaw channel; **l** equivalent canard angle in yaw channel

4.2.4 Simulation and Analysis for the Improved Attitude Controller

In this subsection, the improved attitude controller is simulated under the same conditions used in Sect. 4.2.1. The simulation results are shown in Fig. 3.

As Fig. 3a, b shows, the improved method can also track the desired output precisely, despite it responding slower than that without TD. From Fig. 3c, d, we can see that the sliding surface profile generated by the improved method is flatter. The attitude tracking with reference model attitude is depicted in Fig. 3e, f. From Fig. 3g, h, we can note that the improved method can still respond to the change of lumped uncertainties timely. The transition process arranged by the TD greatly reduces the control commands around the time of reference inputs switching just as Fig. 3i, j shows. Because the improved method generates smaller control commands, the equivalent canard angles needed are smaller, which greatly reduce the burden on the actuator and means a lot to the stability of the system.

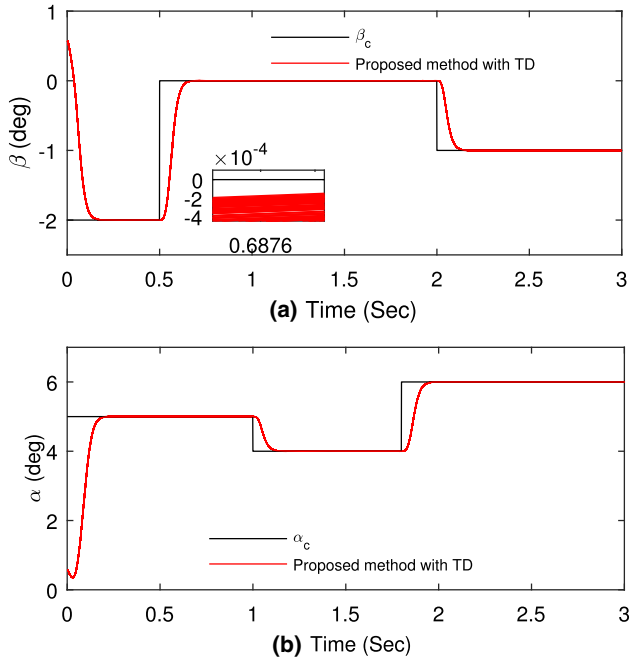

Fig. 4 Attitude tracking of β and α: **a** tracking effect of yaw commands; **b** tracking effect of pitch commands

4.3 Monte Carlo Experiments with Parameter Variation

To demonstrate the robustness of our method, we perform Monte Carlo experiments 100 times. The external disturbance is the same as that in Sect. 4.1. The standard deviation of the error of the aerodynamic parameters is set to be 30% of the nominal value. As Fig. 4 shows, attitude response curve is constrained within a very narrow envelope, which means the proposed control method is insensitive to parameter variation. Figure 5 shows the estimation errors for lumped uncertainty. The curve appears to be ladder shape due to the relatively large sampling period, but it does not prevent the RBF networks from estimating the uncertainties precisely as the figure exhibits.

5 Conclusion

In this paper, an attitude decoupling control strategy is proposed for gliding-guided projectile based on model following SMC and RBF neural network. The coupling inputs are kept as a nominal input instead of being included in lumped uncertainty, so high control value is avoided. Also, control signal jumping phenomenon is avoided by using of TD, which provides a transition process for the reference inputs. The coupling effects have been weakened completely using of RBF network, which is demonstrated by simulations.

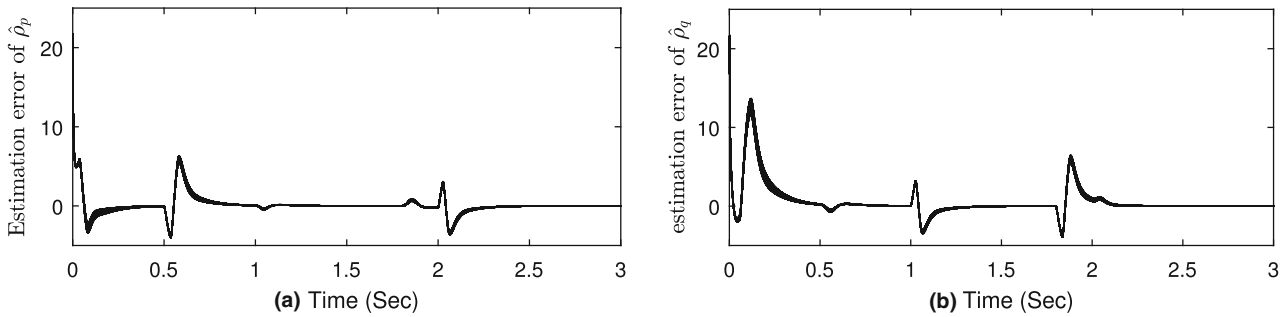

Fig. 5 Estimation errors: **a** lumped uncertainty estimation error of d_p; **b** lumped uncertainty estimation error of d_q

Acknowledgements This work was supported in part of China Postdoctoral Science Foundation under Grant no. 2019M651838.

References

1. Li Y, Yang ZH, Cui NG (2008) A study of optimal trajectory for Boost-glide missile. J Astronaut 29(1):66–71
2. Shi JG, Wang ZY, Cao XB, Zhang BL (2007) Effect of motorial modes of gliding extended range projectile on range extended efficiency. Acta Armament 28(6):651–655
3. Akhtar A, Nielsen C, Waslander SL (2017) Path following using dynamic transverse feedback linearization for Car-Like robots. IEEE Trans Rob 31(2):269–279
4. Li HT, Yang S, Ren HL (2016) Dynamic decoupling control of DGCMG gimbal system via state feedback linearization. Mechatronics 36(2016):127–135
5. Liu C, Liu G, Fang JC (2016) Feedback linearization and extended state observer based control for rotor-AMBs system with mismatched uncertainties. IEEE Trans Industr Electron 64(2):1313–1322
6. Hamzaçebi H, Hömer M (2017) On the periodic gait stability of a multi-actuated spring-mass hopper model via partial feedback linearization. Nonlinear Dyn 88(2):1–20
7. Fang Z (2017) Control of an LLC resonant converter using load feedback linearization. IEEE Trans Power Electron 33(1):887–898
8. Hua CC, Liu G, Zhang L (2017) Cooperative stabilization for linear switched systems with asynchronous switching. IEEE Trans Syst Man Cybern Syst 49(6):1081–1087
9. Hua CC, Liu G, Zhang L (2017) Adaptive fuzzy prescribed performance control for nonlinear switched time-delay systems with unmodeled dynamics. IEEE Trans Fuzzy Syst 26(4):1934–1945
10. Yang RG, Sun MW, Chen ZQ (2010) ADRC—based attitude control optimization and simulation. J Syst Simul 22(11):2689–2693
11. Precup RE (2017) Model-free sliding mode control of nonlinear systems: algorithms and experiments. Inf Sci 381(1):176–192
12. Shibasaki H, Ishida Y (2016) Modified model-following sliding mode control based on the active disturbance rejection control. In: 7th international conference on intelligent systems, modelling and simulation, pp 219–224
13. Liu D, Yang GH (2018) Performance-based data-driven model-free adaptive sliding mode control for a class of discrete-time nonlinear processes. J Process Control 68(2018):186–194
14. Davijani NZ, Jahanfarnia G, Abharian E (2016) Nonlinear fractional sliding mode controller based on reduced order FNPK model for output power control of nuclear research reactors. IEEE Trans Nucl Sci 64(1):713–723
15. Mu B, Zhang K, Shi Y (2017) Integral sliding mode flight controller design for A quadrotor and the application in A heterogeneous multi-agent system. IEEE Trans Industr Electron 64(12):9389–9398
16. Tagne G, Talj R, Charara A (2013) Higher-order sliding mode control for lateral dynamics of autonomous vehicles, with experimental validation. In: 2013 IEEE intelligent vehicles symposium, pp 678–683
17. Wang B (2017) Integral sliding mode flight controller design for A quadrotor and the application in A heterogeneous multi-agent system. IEEE Trans Power Electron 33(9):7927–7937
18. Romdhane H, Dehri K, Nouri AS (2015) Second order sliding mode control for discrete decouplable multivariable systems via input-output models. Int J Autom Comput 12(6):630–638
19. Drakunov SV, Utkin VI (1992) Sliding mode control in dynamic systems. Int J Control 55(4):1029–1037
20. Emel'Yanov SV, Korovin SK, Levant A (1996) High-order sliding modes in control systems. Computat Math Model 7(3):294–318
21. Zhang YX (2007) Artificial neural networks based on principal component analysis input selection for clinical pattern recognition analysis. Talanta 73(1):68–75
22. He W, Chen Y, Zhao Y (2017) Adaptive neural network control of an uncertain robot with full-state constraints. IEEE Trans Cybern 46(3):620–629
23. Tong S (2017) Adaptive neural network output feedback control for stochastic nonlinear systems with unknown dead-zone and unmodeled dynamics. IEEE Trans Cybern 44(6):910–921
24. Luo S (2014) A Chaos RBF dynamics surface control of brushless DC motor with time delay based on tangent barrier Lyapunov function. Nonlinear Dyn 78(2):1193–1204
25. Ak AG, Cansever G (1995) Three link robot control with fuzzy sliding mode controller based on RBF neural network. In: Proceedings of IEEE 14th symposium on mass storage systems, pp 2719–2724
26. Sun Y, Wu CQ (2012) A radial-basis-function network-based method of estimating Lyapunov exponents from a scalar time series for analyzing nonlinear systems stability. Nonlinear Dyn 70(2):1689–1708
27. Song K (2016) On decoupling control of the VGT-EGR system in diesel engines: a new framework. IEEE Trans Control Syst Technol 24(5):1788–1796
28. Talole SE, Phadke SB (2016) Model following sliding mode control based on uncertainty and disturbance estimator. J Dyn Syst Meas Contr 130(3):034501–034505
29. Qian XF, Lin RX, Zhao YN (2008) Missile flight aerodynamics. In: Beijing institute of technology press, pp 90–111
30. Xu QP, Wang X, Wang Z (2018) Design of attitude decoupling controller for gliding guided projectile based on active disturbance rejection control. Syst Eng Electronics 40(2):384–392
31. Yan X, Yang S, Zhang C (2010) Coning motion of spinning missiles induced by the rate loop. J Guid Control Dyn 33(5):1490–1499
32. Ackermann J, Utkin VI (1998) Sliding mode control design based on Ackermann's formula. IEEE Trans Automatic Control 43(2):234–237
33. Salle JL, Lefschetz S (1962) Stability by Liapunov's direct method with applications. Phys Today 15(10):59